Ionics (2017) 23:3545–3554
DOI 10.1007/s11581-017-2158-y

ORIGINAL PAPER

Understanding the photo-electrochemistry of metal-free di and tri substituted thiophene-based organic dyes in dye-sensitized solar cells using DFT/TD-DFT studies

Sudip Mandal[1] · **Shamsher Rao**[1] · **Kothandaraman Ramanujam**[1]

Received: 1 March 2017 / Revised: 17 May 2017 / Accepted: 17 May 2017 / Published online: 4 June 2017

Abstract In this work, two 2, 5-disubstituted and three 2, 3, 5-trisubstituted thiophene-based organic dyes have been investigated using the density functional theory. Although substitution at the 3-position of thiophene ring may retard the back electron transfer, the loss of coplanarity affected the intramolecular charge transfer. The natural bond orbital (NBO) analysis of dye-$(TiO_2)_8$ cluster has been performed to study the feasibility of electron injection. The highest driving force of dye regeneration, higher negative NBO value of cyanoacrylic acid (CA) attached to the $(TiO_2)_8$ cluster (CA-$(TiO_2)_8$ moiety), and reasonably higher open-circuit voltage make (E)-2-cyano-3-(5′-(4-(diphenylamino)phenyl)-[2,2′-bithiophen]-5-yl)acrylic acid (D1) to perform as an effective light harvester in dye-sensitized solar cells. The outcomes of this theoretical study are in good agreement with the experimental data reported.

Keywords Dye-sensitized solar cells · NBO analysis · PDOS · Dye regeneration · Thiophene

Introduction

Over the past decade, environmental problems related to non-renewable energy sources, such as petroleum and coal, have become matters of serious concern due to their negative impact in the atmosphere. Therefore, in the global motif of sustainable development, enormous research endeavors have been devoted to harvest the clean and renewable energy such as wind energy and solar energy [1]. Dye-sensitized solar cells (DSSCs) are perceived as one of the most promising renewable energy source in comparison to that of other clean energy sources. DSSCs have attracted considerable interest since their invention by O'Regan and Grätzel [2, 3] and in particular due to their low manufacturing cost, environment friendliness, and ease of fabrication. In addition, DSSCs exposed the possibility of designing flexible solar cells [4–6]. In DSSC, organic dye/sensitizer is excited by absorption of solar light. The photo-excited electrons of the dye are injected into the conduction band of the semiconductor and prior to charge recombination, the oxidized dye is restored to its neutral state by I^- in the electrolyte solution. The injected electron on the semiconductor passes through the external circuit to the counter electrode, where it reacts with I_3^- to regenerate I^-. For an efficient DSSC, dye sensitizer must absorb strongly the entire visible and near-IR spectrum of the solar radiation. Furthermore, the energy alignment of the lowest unoccupied molecular orbital (LUMO) of the dye with the conduction band of the semiconductor also requires fine-tuning to inject electrons efficiently and the highest occupied molecular orbital (HOMO) of the dye should be lying sufficiently below the energy level of redox couple to regenerate the dye. From the viewpoints of stability and efficiency, ruthenium polypyridine (N719, N3, black dye) [3, 7–12] complexes are the best performing dyes for DSSCs due to their broad absorption in the visible region. Metal-to-ligand charge transfer (MLCT) is responsible for absorption in the visible region in those dyes. To improve the light-harvesting efficiency in the near-IR region of the solar spectrum, some attempts have been made to tune the MLCT absorption band to higher wavelength by modifying the bipyridyl ligand with various substituents [13–15]. By

Electronic supplementary material The online version of this article (doi:10.1007/s11581-017-2158-y) contains supplementary material, which is available to authorized users.

✉ Kothandaraman Ramanujam
rkraman@iitm.ac.in

[1] Department of Chemistry, Indian Institute of Technology Madras, Chennai 600 036, India

employing this approach, although the absorption maximum red-shifted to higher wavelength, the molar absorption coefficient remained still moderate. Some researchers used tandem cells, wherein photoanode captures the most of the visible spectrum and the photocathode captures the red and near-IR region [16–19]. Although this approach resulted in enhancing the open-circuit voltage, the short-circuit current density was limited in comparison to DSSCs. Despite these advances, the rarity of Ru, environmental issues, and high cost of Ru have stimulated researchers to discover cheaper and environment friendly metal-free sensitizers. In general, metal-free dyes contain a donor (D), π-linker, and acceptor (A) groups, respectively, which are called as D-π-A dyes or push-pull molecules. One of the biggest advantage of D-π-A dyes is their abundances and synthesis in few easy steps. The other features of these dyes are (i) higher molar absorption coefficient vis-à-vis metal-based dyes and (ii) tunable absorption in the visible to near-IR region upon suitable molecular engineering. The D-π-A dyes, such as cyanine- [20], hemicyanine- [21], perylene- [22], coumarin- [23], porphyrin- [24, 25], indoline- [26], carbazole- [27], triphenylamine- (TPA) [28–31], pyrene- [32], and phenothiazine [33]-based dyes have been studied and showed satisfactory performances in DSSC. According to the literature, TPA is the most preferred donor moiety due to its tunable electron donating ability. Recently, ferrocenyl substituted TPA [34] and ferrocenyl bisthazole-linked TPA-based molecular system [35] were reported to exhibit power conversion efficiencies (PCE) of 4.96 and 6.33%, respectively. Misra et al. [31] demonstrated the tuning ability of TPA donor moiety by introducing the positional isomers of pyridine. Metal-free organic dyes based on derivatives of carbazole and triphenylamine (TPA), with thiophene-based π-bridge/linker, have exhibited a power conversion efficiency (PCE) up to 12.8%, while using cobalt(III/II) tris(2,2′-bipyridine) as the redox couple [36, 37], which is close to the value achieved with the Ru-based dyes [7, 10, 12]. Highest efficiency reported till date is 14.3%, while employing two metal-free carbazole and modified TPA-carbazole-based dyes (ADEKA-1 and LEG4) with silyl and carboxyl anchoring groups, and cobalt(III/II) tris(1,10-phenanthroline) complex redox electrolyte [38].

Thiophene-based π-linker oligomers and polymers have been widely explored in DSSCs because of their electronic tunability and chemical and environmental stability [39–42]. Although there are plenty of reports using thiophene as a spacer in organic dyes [43–45], use of oligothiophene moiety as spacer is still rare [46–49]. Oligothiophene moiety shows higher electronic conjugation and coplanarity than benzenoid moieties [50, 51]. Therefore, incorporating oligo(2,5-thiophene) as the spacer of dipolar arylamine/cyanoacrylic acid sensitizers have been explored by Thomas et al. [52]. According to Thomas et al. [52], incorporation of arylamine donor at the C2 and C3 positions of thiophene ring hinders the back electron transfer from TiO_2 to the electrolyte through the delocalization of positive charge between C2 and C3 substituents upon electron injection. In the literature, the density functional theory (DFT) [53–56] is widely used to understand the electronic structure and photophysical properties of the dyes. We have employed DFT to those dyes developed by Thomas et al. [52] and calculated their highest occupied molecular orbital (HOMO), lowest unoccupied molecular orbital (LUMO) energies, and the bandgap (E_g, difference between HOMO and LUMO). Time-dependent DFT (TD-DFT) calculations have been performed to get the photophysical properties of excited state geometries such as maximum absorption wavelength, oscillator strength, and percentage contributions of electronic transition from occupied to virtual orbitals. TD-DFT calculation and evaluation of natural bond orbital (NBO) analysis of dye-$(TiO_2)_8$ cluster of these dyes are the main aspect of this present study.

Computational methods

Kohn-Sham DFT calculations have been employed to optimize the ground state geometries of the dyes using Beck's three-parameter hybrid functional combined with Lee, Yang, and Parr correlation functional (B3LYP) with the 6-31G(d,p) basis set [57–59]. The frequency calculations were performed to confirm the stationary nature of the optimized geometries at energy minimum using the same level of theory. The absence of imaginary frequencies confirms that all the dyes are optimized at minimum ground state energy. The Cartesian coordinates of all the optimized geometries have been provided in the supporting information. From the optimized ground state geometry, the HOMO, LUMO, and band gap energy have been evaluated and frontier orbital analysis was carried out for optimized structures. To get insight into the photophysical properties of the dyes, TD-DFT calculations have been performed and the vertical excitation energies, oscillator strengths (f), and the compositions in terms of excitations between occupied and virtual orbitals were calculated from the excited state geometries. The B3LYP functional [59] has been widely employed among the other functional in DSSC-related works [28, 60–63]. However, the B3LYP functional generally underestimates the excitation energies of charge transfer transitions for large π-conjugated systems [32, 64, 65]. Therefore, by taking consideration of long-range correction factor, the coulomb-attenuating method (CAM-B3LYP) functional [66] has been introduced for establishing suitable intramolecular charge transfer (ICT). Polarizable continuum model (PCM) [67, 68] was used to consider the solvent environment effect during the calculation. The geometry optimization of the dyes and TD-DFT calculations were carried out using the Gaussian 09 software suit [69].

To investigate the electron injection mechanism from the dye to the semiconductor interface, the calculations of the prototype model systems (i.e., dye-TiO_2 anatase (101) interface) were implemented using the DMol^3 software [70, 71] in the Materials Studio 2017 version. Cyanoacrylic acid moiety was used as an anchoring group. The geometry optimizations of dye-$(TiO_2)_8$ clusters were carried out using the generalized gradient-correlated approximation (GGA) method of the Perdew-Burke-Ernzerhof (PBE) [72] functional with the double numeric-polarized (DNP) basis set. It is to be noted that the DNP basis set is the highest quality set available in DMol^3, and it is comparable with the 6-31G(d,p) basis set of the same size [73, 74]. The TD-DFT calculations of dye-$(TiO_2)_8$ clusters were performed using the CAM-B3LYP/6-31G(d,p) method in vacuum by taking the ground state DMol^3 optimized geometry.

Results and discussion

Structures of the dyes

The chemical structures of the five dyes (D1 to D5) are shown in Fig. 1a. The optimized geometries of the five dyes were obtained using the B3LYP/6-31G(d,p) method and presented in Fig. S1, and their corresponding frequency analyses have been shown in Fig. S2. Similarly, the optimized geometry of the dye-$(TiO_2)_8$ clusters are given in Fig. 1b. In all the dyes, TPA and cyanoacrylic acid (CA) act as donor and acceptor, respectively, and thiophene is used as spacer moiety between TPA and CA. D1 and D2 are 2, 5-disubstituted thiophene-based dyes and D3 to D5 contain 2, 3, 5-trisubstituted thiophene-based congeners. The C2 and C3 positions of the thiophene ring are substituted with thiophene-TPA moiety. D1, D2-D3, D4, and D5 contain 2, 3, 4, and 5 thiophene spacers in total. The IUPAC name of the five dyes is presented in Table S1.

Energy level alignment and dye regeneration kinetics

The calculated energy of HOMO (E_{HOMO}), LUMO (E_{LUMO}), and E_g of all five dyes are summarized in Table 1 using the B3LYP/6-31G(d,p) method. The experimental E_{HOMO}, E_{LUMO}, and E_g values, taken from the work of Thomas et al. [52], are given in the parenthesis next to the theoretical values for comparison. However, it is to be noted that solid-state packing effects are not included in the DFT calculations, which tend to affect the HOMO and LUMO energy levels in a thin film compared to an isolated molecule as considered in the calculations. In spite of that, the energy of HOMO and LUMO values estimated is reasonably close to the experimental values. The energy level diagram of all five dyes along with the conduction band (CB) energy level of TiO_2 and redox potential energy of I_3^-/I^- redox electrolyte (−4.8 eV vs. vacuum) [75] is shown in Fig. 2. The energy of the LUMOs of all five dyes lie above the CB of TiO_2 (−4.0 eV vs. vacuum) [76, 77], resulting in an effective electron injection from the

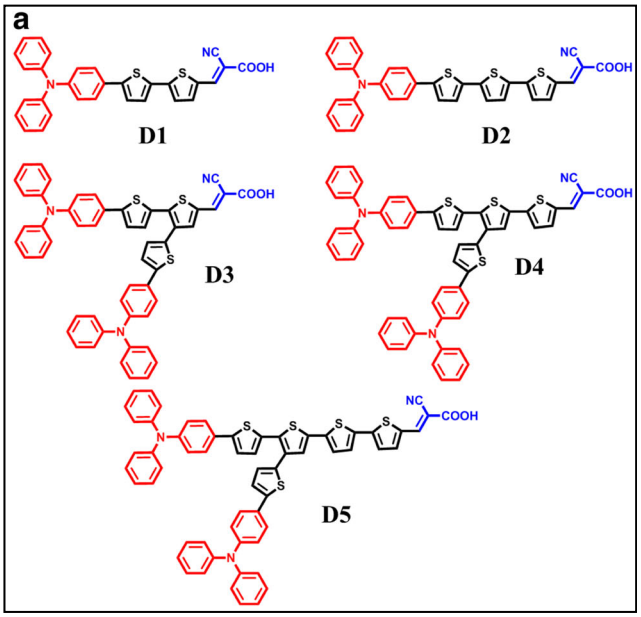

Fig. 1 **a** The chemical structures of the dyes (D1 to D5). **b** The optimized geometries of dye-$(TiO_2)_8$ cluster of the dye (D1 to D4)

Table 1 The calculated HOMO, LUMO, bandgap energy, and driving force for dye regeneration (in eV) of five dyes obtained using the B3LYP/6-31G(d,p) method. The experimentally measured values [1] are given in the parenthesis

Dyes	E_{HOMO}/eV	E_{LUMO}/eV	E_g/eV	Driving force for dye regeneration ($E_{I_3^-/I^-} - E_{HOMO}$)/eV
D1	−5.05 (−4.99)	−2.80 (−2.79)	2.25 (2.20)	0.25
D2	−4.96 (−4.93)	−2.88 (−2.76)	2.08 (2.17)	0.16
D3	−4.97 (−4.99)	−2.80 (−2.81)	2.17 (2.18)	0.17
D4	−4.90 (−4.96)	−2.86 (−2.80)	2.04 (2.16)	0.10
D5	−4.87 (−4.93)	−2.89 (−2.77)	1.98 (2.16)	0.07

LUMO of the dye into the CB of TiO_2. Likewise, the energy of the HOMOs of all five dyes is located below the energy level of the I_3^-/I^- redox electrolyte. However, for regeneration of the oxidized dye, the sufficient driving force ($E_{I_3^-/I^-} - E_{HOMO}$) is required and the calculated values of "$E_{I_3^-/I^-} - E_{HOMO}$ '" were tabulated in Table 1. The maximum and minimum driving force for dye regeneration were found for D1 (0.25 eV) and D5 (0.07 eV), respectively. It is important to have sufficient driving force for dye regeneration as it can influence the back electron transfer kinetics between the injected electrons in the CB of TiO_2 with the oxidized dye and I_3^-. The decreasing order of the driving force of dye regeneration energy is D1 > D3 > D2 > D4 > D5. It is palpable from Fig. 2 that D4 and D5 offer very less driving force for dye regeneration kinetics as compared with the other three dyes. The relative position of HOMO of D1 to D3 is sufficiently negative to that of the redox energy of the electrolyte, thereby enhancing the chance of dye regeneration. Experimentally, D1 is clearly seen as the best performing dye in DSSC with an efficiency of 6.15% [52].

Projected density of state analysis

The projected density of state (PDOS) calculation has been carried out for all five dyes using the B3LYP/6-31G(d,p) method. PDOS analysis offers a qualitative information about electron density of dyes at different moieties such as donor, π-linker, and acceptor. The presence of ICT in the dyes during photoexcitation can be explained by examining the HOMO and LUMO of dyes, i.e., the relative ordering of occupied and virtual orbitals. During photoexcitation, the charge transfer occurs from the donor moiety to the acceptor moiety as the PDOS in the donor shift to the acceptor located on the virtual orbital (LUMO). It is crucial for ICT that the HOMO must localize on the donor moiety and the LUMO must localize on the acceptor moiety. Figure 3 presents the plot of the PDOS of the donor, π-linker, and acceptor for the five dyes at HOMO and LUMO. It is seen that for all five dyes, the electron density on HOMO (55 to 70% in donor and 25 to 44% in π-linker) shifts to LUMO (52 to 63% in π-linker and 36 to 43% in acceptor). This indicates that during ICT, there is some amount of electron retention on the π-linker moiety which is well agreed to the frontier orbital diagram of dyes shown in Fig. 4.

Natural bond orbital analysis of dye-$(TiO_2)_8$ cluster

Furthermore, natural bond orbital (NBO) analysis was performed using the ground state geometry of all the five dyes to confirm the direction of the flow of electron in photoanode. Generally, the positive NBO value indicates the electron donating ability and negative NBO value about the electron accepting ability of a group. The NBO values of the donor, π-linker, and acceptor have increased in THF as compared to vacuum. In order to get the NBO charges in solvent medium, the polarized continuum model (PCM) is used. This method creates the solute cavity via a set of overlapping spheres and which stabilizes the dye molecules. Therefore, the polarity of the dye molecule increased in THF as compared with vacuum. Table S2 compares the NBO values obtained in THF and vacuum. The positive NBO value of TPA and negative NBO value of CA indicate TPA and CA to be effective electron donor and acceptor, respectively. Therefore, for all five dyes, the charge separation state can be established upon photoexcitation and the electron can be shifted from TPA to the CA part via ICT.

The direction of electron flow in a DSSC device is from dye to the CB of semiconductor. Hence, to get insight into the electron transfer mechanism at the dye-TiO_2 interface, NBO analysis of the dye-$(TiO_2)_8$ cluster was performed by employing the

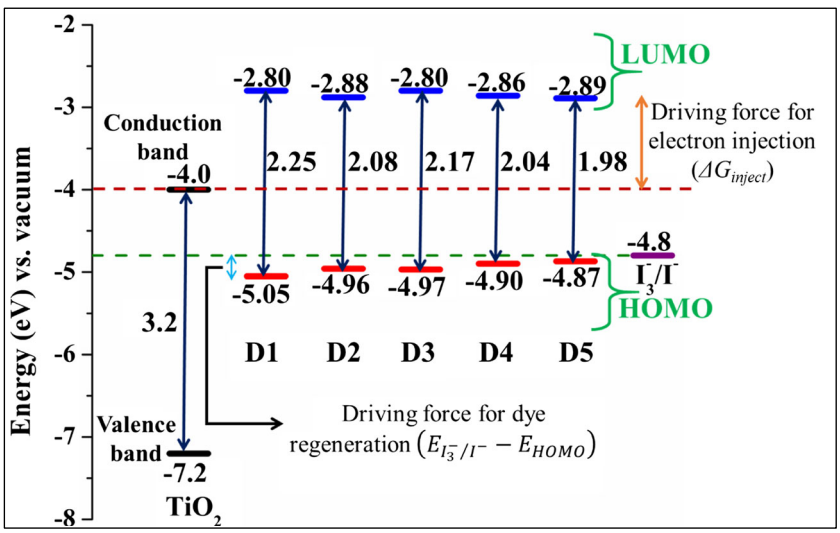

Fig. 2 The energy level diagram of five dyes including the conduction band of TiO_2 and redox potential energy level of I_3^-/I^- couple

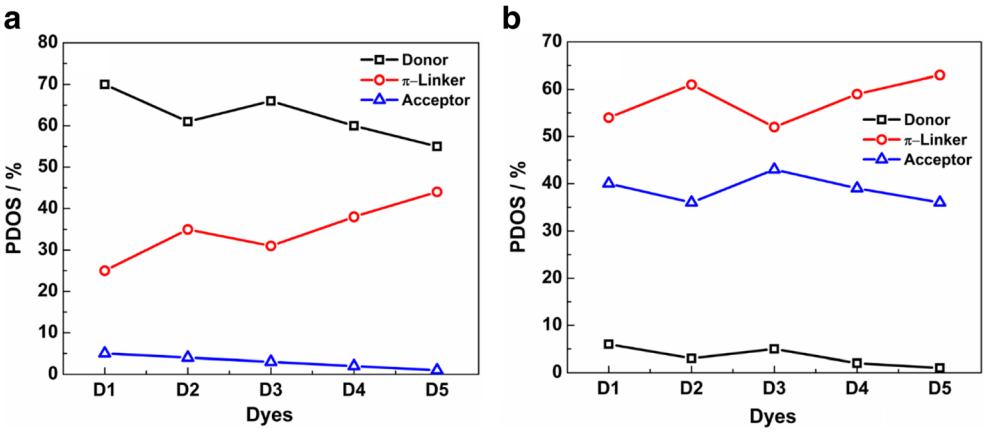

Fig. 3 The projected density of states (PDOS) plot of the five dyes at **a** HOMO and **b** LUMO

ground state optimized structure obtained using the B3LYP/6-31G(d,p) method. Figure 5 shows the frontier orbital diagram of the dye-$(TiO_2)_8$ cluster. The NBO values of the dye-$(TiO_2)_8$ cluster are summarized in Table 2. The positive NBO values are observed for TPA and π-linker moieties and negative NBO values are noticed for CA-$(TiO_2)_8$ moiety. The reasonable higher negative NBO values on CA-$(TiO_2)_8$ moiety have been observed for D1 (−0.657), D3 (−0.655), and D4 (−0.642), which indicates the possibility of electron injection from the LUMO of the dye to the CB of the TiO_2. D2 and D5 are having the least NBO value at the CA-$(TiO_2)_8$ moiety, indicating poor electron injection into the CB of TiO_2. Therefore, D1, D3, and D4 would show higher power conversion efficiency as compared to D2 and D5, which is correlating perfectly with the experimental data [52] (experimental order of the efficiency of DSSCs made of those dyes: D1 > D4 > D3 > D2 > D5). Hence, based on the ($E_{I_3^-/I^-} - E_{HOMO}$) and NBO value at CA-$(TiO_2)_8$ moiety, the expected order of performance of the dyes is D1 > D3 > D4 > D2 > D5.

UV-vis absorption spectra

TD-DFT calculation has been carried out to get insight into the photophysical properties of the dyes using the CAM-B3LYP/6-31G(d,p) method. The simulated UV-Vis absorption spectra in THF solvent are displayed in Fig. 6 by considering 30 lowest singlet-singlet (S_0 to S_1) transitions. The simulated

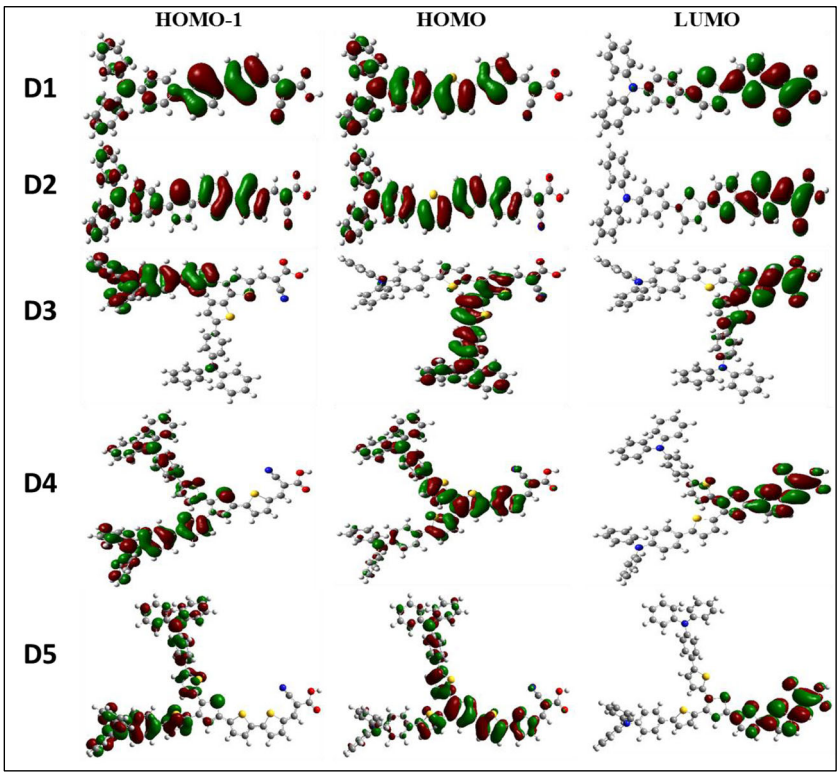

Fig. 4 Frontier molecular orbitals (HOMO-1 to LUMO) of D1 to D5 obtained using the B3LYP/6-31G(d,p) method

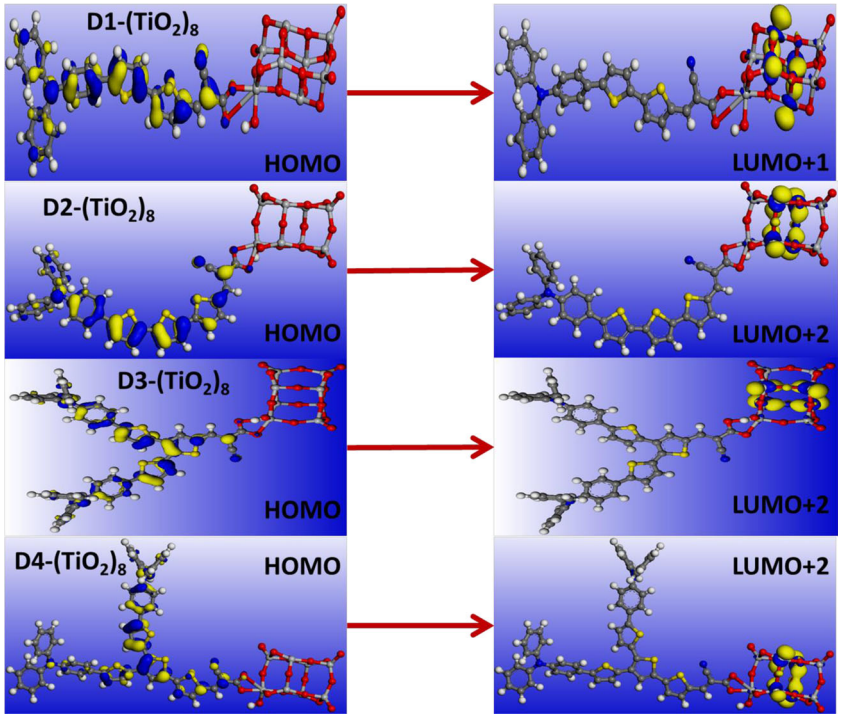

Fig. 5 Frontier orbital diagram of dye-$(TiO_2)_8$ cluster

UV-Vis absorption spectra show the reasonable agreement with the experimentally observed absorption spectra reported by Thomas et al. [52]. The comparison of the experimental and simulated absorption spectra has been shown in Fig. S3. The first band around 200–400 nm corresponds to π-π* transition for D1 and D2. For example, electron density, both in HOMO and LUMOs (LUMO + 1, LUMO + 3 and LUMO + 4), are almost on the donor part (Fig. S4(a)) for D1. For D3 to D5, this band is overlapped with the ICT band (400–700 nm). The extent of overlap of the π-π* band with the ICT band, in three substituted dyes, is more for D4 and D5 than D3. This overlaps indicates the possibility of π-π* transition influencing the ICT transition in the excited state of the dyes. For example, the frontier orbital diagram of D4 corresponding to the oscillator at 273, 305, and 342 nm are shown in Fig. S4(b). This clearly shows the presence of electron clouds on the donor and π-linker both in ground and excited states. From Fig. 6, it can be seen that the aforementioned π-π* transition band intensity is more for D3 to D5 than D1 and D2, which is due to the addition of the extra substituent at the C3 position of the 2,3-substituted thiophene ring. The larger extinction coefficient of the ICT band in D1 than in D3 (or in D2 than in D4) may be attributed due to the loss in coplanarity between the electron donor (at the C2 position of the thiophene) and the electron acceptor because of the presence of the C3 substituent. The photophysical properties such as computed maximum wavelength (λ_c, in nm), experimentally observed maximum wavelength (λ_{max}, in nm), oscillator strength (f), and the percentage of the major transitions are presented in Table S3. The λ_c (in THF solvent) of D1 to D5 are 473, 494, 470, 478, and 490 nm, respectively, which show a close

Table 2 The natural bond orbital (NBO) analysis of five dye-$(TiO_2)_8$ cluster obtained using the B3LYP/6-31G(d,p) method

Dye-$(TiO_2)_8$	Donor (TPA)	π-Linker (thiophene)	Acceptor (CA-$(TiO_2)_8$)
D1-$(TiO_2)_8$	0.192	0.180	−0.657
D2-$(TiO_2)_8$	0.172	0.340	−0.468
D3-$(TiO_2)_8$	0.163	0.176	−0.655
D4-$(TiO_2)_8$	0.770	0.149	−0.642
D5-$(TiO_2)_8$	0.665	0.153	−0.186

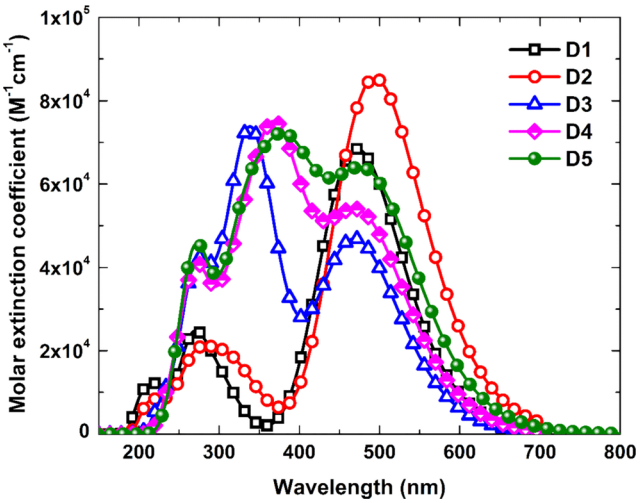

Fig. 6 Computed UV-Vis absorption spectra of five dyes in THF solvent obtained using the CAM-B3LYP/6-31G(d,p) method

match to the λ_{max} of the experimentally observed values [52]. The blue-shift in λ_c of D3 and D4 as compared with D1 and D2 is ascribed due to the loss in coplanarity, which hinders the ICT, by addition of the substituent at the C3 position. The percentage transition ascribed to HOMO to LUMO is maximum for D1 (70%) among all the dyes. The TD-DFT calculations of dye-$(TiO_2)_8$ cluster were performed to get the UV-Vis absorption spectra of the five dyes using the CAM-B3LYP/6-31G(d,p) method in vacuum. The simulated UV-Vis absorption spectra of dye-$(TiO_2)_8$ cluster are shown in Fig. S5. The spectra show a dramatic red shift as compared to the spectra obtained in solvent medium due to the increased delocalization of the π* orbital of the conjugated framework caused by the interaction between the carboxylate group and the Ti^{4+} ions [78]. The higher *f* for D1 and higher driving force for dye regeneration coupled with high NBO value of CA-$(TiO_2)_8$ moiety steers D1 to perform better in DSSC.

Calculation of photovoltaic parameters pertain to DSSCs' performance

Light-harvesting efficiency (LHE (λ)) [79] at a particular wavelength (associated with oscillator strength, *f*) is provided in Eq. 1:

$$\mathrm{LHE} = 1-10^{-f} \tag{1}$$

Φ_{inject}, the electron injection efficiency is proportional to the *f* and free energy of electron injection (ΔG_{inject}) which is expressed by [80]:

$$\Phi_{inject} \propto f\left(\Delta G_{inject}\right) \tag{2}$$

Therefore, higher negative value of ΔG_{inject} corresponds to greater electron injection efficiency. ΔG_{inject} can be calculated as the difference between excited state oxidation potential ($E_{OX}^{dye^*}$) of the dye and the ground state reduction potential (E_{CB}) (Table 3) of the conduction band (CB) of the TiO_2 (E_{CB} = −4.0 eV [76]) and is expressed by [65]:

$$\Delta G_{inject} = E_{OX}^{dye^*} - E_{CB} \tag{3}$$

$E_{OX}^{dye^*}$ can be estimated using Eq. 4:

$$E_{OX}^{dye^*} = E_{OX}^{dye} - \Delta E \tag{4}$$

where E_{OX}^{dye} (i.e., $-E_{HOMO}$) is the ground state oxidation potential of the dye [81] and ΔE is the electronic vertical transition energy associated with the λ_{max} (Table 3).

ΔG_{inject} and LHE values are presented in Table 3. All the dyes displayed sufficient exergonicity as the calculated ΔG_{inject} values were negative (process to occur spontaneously), which is facilitating the electron injection from E_{LUMO} of the dye to the CB of TiO_2. LHE is also more than 90% for all the dyes considered in this study, i.e., all dyes can be able to harvest light to generate electricity. Scharber et al. [82] carefully analyzed a series of organic solar cell devices employing 26 polymer donor moieties having a common acceptor and different HOMO levels. Based on their study, they have proposed an empirical equation (Eq. 5). It is to be noted that the V_{OC} loss of 0.3 V indicated is empirical and the actual loss could be greater or smaller than 0.3 V. In this study, we have chosen 0.3 V to predict the trend in the V_{OC} variation among the five dyes studied and the emphasis is not on finding the exact V_{OC} values [35]:

$$V_{OC} = |E_{HOMO}(\text{donor or dye})| - |E_{LUMO}(\text{acceptor}) \text{of } TiO_2| - 0.3 \tag{5}$$

The calculated V_{OC} are presented in Table 3. The decreasing order of V_{OC} is D1 > D3 > D2 > D4 > D5. Please note, our model does not consider the kinetics of back electron transfer; hence, the calculated V_{OC} are only an indicative value, depending upon the dye molecule's size and substitution that they bear the extent of back electron transfer kinetics may vary. Experimentally, D3 and D4 showed a higher V_{OC} value than D1, because of the effect of substitution at the C3 position of the thiophene ring, which may retard the back electron transfer, hence improving the open-circuit voltage. Therefore, it can be concluded that D1 is the best performing dye in DSSC, due to the highest driving force of dye regeneration and the highest negative NBO value of CA-$(TiO_2)_8$ moiety coupled with reasonably higher open-circuit voltage.

Table 3 The calculated excited and ground state oxidation potential ($E_{OX}^{dye^*}$ and E_{OX}^{dye}), the electronic vertical transition energy (ΔE) associated with the λ_{max}, LHE, ΔG_{inject}, and open-circuit voltage (V_{OC}) of the dyes

Dye	λ_{max}/nm	ΔE/eV	$E^{dye}{}_{OX}$/eV	$E^{dye*}{}_{OX}$/eV	ΔG_{inject}/eV	LHE	V_{OC}/V (theo)	V_{OC}/V (expt)
D1	473	2.62	5.05	2.43	−1.57	0.979	0.75	0.63
D2	494	2.51	4.96	2.45	−1.55	0.992	0.66	0.61
D3	470	2.64	4.97	2.33	−1.67	0.928	0.67	0.68
D4	478	2.59	4.90	2.31	−1.69	0.944	0.60	0.65
D5	490	2.53	4.87	2.34	−1.66	0.963	0.57	0.61

Conclusions

The dyes comprising of oligothiophene as spacers, TPA as donor at C2- and C3-sites of thiophene, and cyanoacrylic acid as acceptor have been investigated by using the B3LYP/6-31G(d,p) method and the UV-Vis absorption spectra have been simulated by using the TD-DFT methods with the PCM model to simulate the solvent environment. Although, substitution at the 3-position of the thiophene ring may retard the back electron transfer, the loss of coplanarity affected the intramolecular charge transfer. The electron injection is possible by all five dyes as the LUMO of all the dyes are above the CB of TiO_2, indicating a thermodynamically favorable charge transfer from the dyes to the CB of the TiO_2. The NBO analysis of the dye-$(TiO_2)_8$ cluster showed that the higher negative NBO value of the dye-$(TiO_2)_8$ cluster for D1 indicates feasibility of intermolecular charge transfer from the TPA moiety to the CB of TiO_2. The highest driving force for dye regeneration and higher NBO value of CA-$(TiO_2)_8$ moiety coupled with reasonable higher open-circuit voltage make D1 to be the clear winner among all the dyes studied for the DSSC application. The outcomes of this theoretical study are clearly explaining the experimental data obtained. Hence, the reason behind the poor performance of D2 and D5 is their poor electron injection ability.

Acknowledgements The high-performance computer center at IIT Madras is gratefully acknowledged for the computer time and computing facility. We thank Prof. Matsumi and Dr. Raman from JAIST, Japan, for extending the supercomputing facility which pertain to the study of dye-$(TiO_2)_8$ interface.

References

1. Ali Tahir A, Ullah H, Sudhagar P, Asri Mat Teridi M, Devadoss A, Sundaram S (2016) The application of graphene and its derivatives to energy conversion, storage, and environmental and biosensing devices. Chem rec 16(3):1591–1634
2. O'Regan B, Gratzel M (1991) A low-cost, high-efficiency solar cell based on dye-sensitized colloidal TiO_2 films. Nature 353(6346): 737–740
3. Nazeeruddin MK, Pechy P, Renouard T, Zakeeruddin SM, Humphry-Baker R, Comte P et al (2001) Engineering of efficient panchromatic sensitizers for nanocrystalline TiO_2-based solar cells. J am Chem Soc 123(8):1613–1624
4. Kuang D, Brillet J, Chen P, Takata M, Uchida S, Miura H et al (2008) Application of highly ordered TiO_2 nanotube arrays in flexible dye-sensitized solar cells. ACS Nano 2(6):1113–1116
5. Ito S, Rothenberger G, Liska P, Comte P, Zakeeruddin SM, Péchy P et al (2006) High-efficiency (7.2%) flexible dye-sensitized solar cells with Ti-metal substrate for nanocrystalline-TiO_2 photoanode. Chem Commun (Cambridge, U K). 38:4004–4006.
6. Fan X, Chu Z, Wang F, Zhang C, Chen L, Tang Y et al (2008) Wire-shaped flexible dye-sensitized solar cells. Adv Mater (Weinheim, Ger) 20(3):592–595
7. Nazeeruddin MK, De Angelis F, Fantacci S, Selloni A, Viscardi G, Liska P et al (2005) Combined experimental and DFT-TDDFT computational study of photoelectrochemical cell ruthenium sensitizers. J am Chem Soc 127(48):16835–16847
8. Chiba Y, Islam A, Watanabe Y, Komiya R, Koide N, Han L (2006) Dye-sensitized solar cells with conversion efficiency of 11.1%. Jpn J Appl Phys 45(7L):L638
9. Grätzel M (2004) Conversion of sunlight to electric power by nanocrystalline dye-sensitized solar cells. J Photochem Photobiol a Chem 164(1):3–14
10. Nazeeruddin MK, Kay A, Rodicio I, Humphry-Baker R, Mueller E, Liska P et al (1993) Conversion of light to electricity by charge-transfer sensitizers on nanocrystalline TiO_2 electrodes. J am Chem Soc 115:6382–6390
11. Nazeeruddin MK, Splivallo R, Liska P, Comte P, Grätzel M (2003) A swift dye uptake procedure for dye sensitized solar cells. Chem Commun (Cambridge, U K) 12:1456–1457.
12. Nazeeruddin MK, Pechy P, Grätzel M (1997) Efficient panchromatic sensitization of nanocrystalline TiO_2 films by a black dye based on a trithiocyanato–ruthenium complex. Chem Commun (Cambridge, U K) 18:1705–1706.
13. Hagfeldt A, Boschloo G, Sun L, Kloo L, Pettersson H (2010) Dye-sensitized solar cells. Chem rev 110(11):6595–6663
14. Klein C, Nazeeruddin MK, Liska P, Di Censo D, Hirata N, Palomares E et al (2005) Engineering of a novel ruthenium sensitizer and its application in dye-sensitized solar cells for conversion of sunlight into electricity. Inorg Chem 44(2):178–180
15. Funaki T, Funakoshi H, Kitao O, Onozawa-Komatsuzaki N, Kasuga K, Sayama K et al (2012) Cyclometalated ruthenium (II) complexes as near-IR sensitizers for high efficiency dye-sensitized solar cells. Angew Chem Int Ed 51(30):7528–7531
16. Powar S, Bhargava R, Daeneke T, Götz G, Bäuerle P, Geiger T et al (2015) Thiolate/disulfide based electrolytes for p-type and tandem dye-sensitized solar cells. Electrochim Acta 182:458–463
17. Nattestad A, Mozer AJ, Fischer MK, Cheng Y-B, Mishra A, Bäuerle P et al (2010) Highly efficient photocathodes for dye-sensitized tandem solar cells. Nat Mater 9(1):31–35
18. Odobel F, Pellegrin Y, Anne FB, Jacquemin D (2014) Molecular engineering of efficient dyes for p-type semiconductor sensitization. In high-efficiency solar cells. Springer International Publishing, Switzerland, Chapter 8, pp. 215–246.
19. Gibson EA, Smeigh AL, Le Pleux L, Fortage J, Boschloo G, Blart E et al (2009) A p-type NiO-based dye-sensitized solar cell with an open-circuit voltage of 0.35 V. Angew Chem 121(24):4466–4469
20. Ehret A, Stuhl L, Spitler M (2001) Spectral sensitization of TiO~ 2 nanocrystalline electrodes with aggregated cyanine dyes. J Phys Chem B 105(41):9960–9965
21. Chen Y-S, Li C, Zeng Z-H, Wang W-B, Wang X-S, Zhang B-W (2005) Efficient electron injection due to a special adsorbing group's combination of carboxyl and hydroxyl: dye-sensitized solar cells based on new hemicyanine dyes. J Mater Chem 15(16):1654–1661
22. Shibano Y, Umeyama T, Matano Y, Imahori H (2007) Electron-donating perylene tetracarboxylic acids for dye-sensitized solar cells. Org Lett 9(10):1971–1974
23. Hara K, Kurashige M, Dan-oh Y, Kasada C, Shinpo A, Suga S et al (2003) Design of new coumarin dyes having thiophene moieties for highly efficient organic-dye-sensitized solar cells. New J Chem 27(5):783–785
24. Yella A, Lee H-W, Tsao HN, Yi C, Chandiran AK, Nazeeruddin MK et al (2011) Porphyrin-sensitized solar cells with cobalt (II/III)–based redox electrolyte exceed 12 percent efficiency. Science 334(6056):629–634
25. Mathew S, Yella A, Gao P, Humphry-Baker R, Curchod BF, Ashari-Astani N et al (2014) Dye-sensitized solar cells with 13% efficiency achieved through the molecular engineering of porphyrin sensitizers. Nature Chem 6(3):242–247

26. Horiuchi T, Miura H, Sumioka K, Uchida S (2004) High efficiency of dye-sensitized solar cells based on metal-free indoline dyes. J am Chem Soc 126(39):12218–12219
27. Teng C, Yang X, Yuan C, Li C, Chen R, Tian H et al (2009) Two novel carbazole dyes for dye-sensitized solar cells with open-circuit voltages up to 1 V based on Br^-/Br_3^- electrolytes. Org Lett 11(23): 5542–5545
28. Mandal S, Kushwaha S, Mukkamala R, Siripina VK, Aidhen IS, Rajakumar B et al (2016) Metal-free bipolar/octupolar organic dyes for DSSC application: a combined experimental and theoretical approach. Org Electron 36:177–184. doi:10.1016/j.orgel.2016.06.009
29. Xu W, Peng B, Chen J, Liang M, Cai F (2008) New triphenylamine-based dyes for dye-sensitized solar cells. J Phys Chem C 112(3):874–880
30. Li G, Jiang K-J, Li Y-F, Li S-L, Yang L-M (2008) Efficient structural modification of triphenylamine-based organic dyes for dye-sensitized solar cells. J Phys Chem C 112(30):11591–11599
31. Misra R, Maragani R, Arora D, Sharma A, Sharma GD (2016) Positional isomers of pyridine linked triphenylamine-based donor-acceptor organic dyes for efficient dye-sensitized solar cells. Dyes Pigments 126:38–45
32. Baheti A, Lee C-P, Thomas KJ, Ho K-C (2011) Pyrene-based organic dyes with thiophene containing π-linkers for dye-sensitized solar cells: optical, electrochemical and theoretical investigations. Phys Chem Chem Phys 13(38):17210–17221
33. Kim SH, Kim HW, Sakong C, Namgoong J, Park SW, Ko MJ et al (2011) Effect of five-membered heteroaromatic linkers to the performance of phenothiazine-based dye-sensitized solar cells. Org Lett 13(21):5784–5787
34. Misra R, Maragani R, Patel K, Sharma G (2014) Synthesis, optical and electrochemical properties of new ferrocenyl substituted triphenylamine based donor–acceptor dyes for dye sensitized solar cells. RSC Adv 4(66):34904–34911
35. Maragani R, Misra R, Roy M, Singh MK, Sharma GD (2017) $(D–\pi–A)_2–\pi–D–A$ type ferrocenyl bisthiazole linked triphenylamine based molecular systems for DSSC: synthesis, experimental and theoretical performance studies. Phys Chem Chem Phys 19:8925–8933
36. Kakiage K, Aoyama Y, Yano T, Otsuka T, Kyomen T, Unno M et al (2014) An achievement of over 12 percent efficiency in an organic dye-sensitized solar cell. Chem Commun (Cambridge, U K) 50(48):6379–6381
37. Zhang M, Wang Y, Xu M, Ma W, Li R, Wang P (2013) Design of high-efficiency organic dyes for titania solar cells based on the chromophoric core of cyclopentadithiophene-benzothiadiazole. Energy Environ Sci 6(10):2944–2949
38. Kakiage K, Aoyama Y, Yano T, Oya K, Fujisawa J-I, Hanaya M et al (2015) Chem Commun (Cambridge, U K) 51(88):15894–15897
39. Granström M, Petritsch K, Arias A, Lux A, Andersson M, Friend R (1998) Laminated fabrication of polymeric photovoltaic diodes. Nature 395(6699):257–260
40. Camaioni N, Garlaschelli L, Geri A, Maggini M, Possamai G, Ridolfi G (2002) Solar cells based on poly (3-alkyl) thiophenes and [60] fullerene: a comparative study. J Mater Chem 12(7): 2065–2070
41. Cremer J, Mena-Osteritz E, Pschierer NG, Müllen K, Bäuerle P (2005) Dye-functionalized head-to-tail coupled oligo (3-hexylthiophenes)—perylene–oligothiophene dyads for photovoltaic applications. Org Biomol Chem 3(6):985–995
42. Sivula K, Luscombe CK, Thompson BC, Fréchet JM (2006) Enhancing the thermal stability of polythiophene: fullerene solar cells by decreasing effective polymer regioregularity. J am Chem Soc 128(43):13988–13989
43. Fischer MK, Wenger S, Wang M, Mishra A, Zakeeruddin SM, Grätzel M et al (2010) D-π-A sensitizers for dye-sensitized solar cells: linear vs branched oligothiophenes. Chem Mater 22(5):1836–1845
44. Miyazaki E, Okanishi T, Suzuki Y, Ishine N, Mori H, Takimiya K et al (2011) Simple oligothiophene-based dyes for dye-sensitized solar cells (DSSCs): anchoring group effects on molecular properties and solar cell performance. Bull Chem Soc Jpn 84(5):459–465
45. Feng Q, Zhang Q, Lu X, Wang H, Zhou G, Wang Z-S (2013) Facile and selective synthesis of oligothiophene-based sensitizer isomers: an approach toward efficient dye-sensitized solar cells. ACS Appl Mater Interfaces 5(18):8982–8990
46. Hara K, Wang Z-S, Sato T, Furube A, Katoh R, Sugihara H et al (2005) Oligothiophene-containing coumarin dyes for efficient dye-sensitized solar cells. J Phys Chem B 109(32):15476–15482
47. Koumura N, Wang Z-S, Mori S, Miyashita M, Suzuki E, Hara K (2006) Alkyl-functionalized organic dyes for efficient molecular photovoltaics. J am Chem Soc 128(44):14256–14257
48. Choi H, Lee JK, Song KH, Song K, Kang SO, Ko J (2007) Synthesis of new julolidine dyes having bithiophene derivatives for solar cell. Tetrahedron 63(7):1553–1559
49. Kim D, Lee JK, Kang SO, Ko J (2007) Molecular engineering of organic dyes containing N-aryl carbazole moiety for solar cell. Tetrahedron 63(9):1913–1922
50. Cheng LT, Tam W, Stevenson SH, Meredith GR, Rikken G, Marder SR (1991) Experimental investigations of organic molecular nonlinear optical polarizabilities. 1. Methods and results on benzene and stilbene derivatives. J Phys Chem 95(26):10631–10643
51. Hansch C, Leo A, Taft R (1991) A survey of Hammett substituent constants and resonance and field parameters. Chem rev 91(2):165–195
52. Justin Thomas K, Hsu Y-C, Lin JT, Lee K-M, Ho K-C, Lai C-H et al (2008) 2, 3-Disubstituted thiophene-based organic dyes for solar cells. Chem Mater 20(5):1830–1840
53. Narra VK, Ullah H, Singh VK, Giribabu L, Senthilarasu S, Karazhanov SZ et al (2015) D–π–A system based on zinc porphyrin dyes for dye-sensitized solar cells: combined experimental and DFT–TDDFT study. Polyhedron 100:313–320
54. Ullah H, Bibi S, Tahir AA, Mallick TK (2017) Donor-acceptor polymer for the design of all-solid-state dye-sensitized solar cells. J Alloys Compd 696:914–922
55. Ullah H (2017) Inter-molecular interaction in Polypyrrole/TiO 2: a DFT study. J Alloys Compd 692:140–148
56. Ullah H, Tahir AA, Mallick TK (2017) Polypyrrole/TiO_2 composites for the application of photocatalysis. Sensors Actuators B Chem 241:1161–1169
57. Pople JA, Gill PM, Johnson BG (1992) Kohn—Sham density-functional theory within a finite basis set. Chem Phys Lett 199(6): 557–560
58. Becke AD (1993) Density-functional thermochemistry. III. The role of exact exchange. J Chem Phys 98(7):5648–5652
59. Lee C, Yang W, Parr RG (1988) Development of the Colle-Salvetti correlation-energy formula into a functional of the electron density. Phys rev B 37(2):785
60. Mandal S, Ramanujam K (2016) DFT/TD-DFT studies of metal-free N-annulated perylene based organic sensitizers for dye-sensitized solar cells: is thiophene spacer essential for improving the DSSC performance? ChemistrySelect 1(18):5854–5862
61. Al-Sehemi AG, Irfan A, Asiri AM, Ammar YA (2012) Synthesis, characterization and DFT study of methoxybenzylidene containing chromophores for DSSC materials. Spectrochim Acta a Mol Biomol Spectrosc 91:239–243
62. Sirohi R, Kim DH, Yu S-C, Lee SH (2012) Novel di-anchoring dye for DSSC by bridging of two mono anchoring dye molecules: a conformational approach to reduce aggregation. Dyes Pigments 92(3):1132–1137
63. Sun LL, Zhang T, Wang J, Li H, Yan LK, Su ZM (2015) Exploring the influence of electron donating/withdrawing groups on hexamolybdate-based derivatives for efficient p-type dye-sensitized solar cells (DSSCs). RSC Adv 5(50):39821–39827

64. Shimogawa H, Endo M, Taniguchi T, Nakaike Y, Kawaraya M, Segawa H et al (2017) D–π–A dyes with an intramolecular B–N coordination bond as a key scaffold for electronic structural tuning and their application in dye-sensitized solar cells. Bull Chem Soc Jpn 90(4):441–450
65. Zhang J, Kan Y-H, Li H-B, Geng Y, Wu Y, Su Z-M (2012) How to design proper π-spacer order of the D-π-A dyes for DSSCs? A density functional response. Dyes Pigments 95(2):313–321. doi: 10.1016/j.dyepig.2012.05.020
66. Yanai T, Tew DP, Handy NC (2004) A new hybrid exchange–correlation functional using the coulomb-attenuating method (CAM-B3LYP). Chem Phys Lett 393(1):51–57
67. Cossi M, Rega N, Scalmani G, Barone V (2003) Energies, structures, and electronic properties of molecules in solution with the C-PCM solvation model. J Comput Chem 24(6):669–681
68. Takano Y, Houk K (2005) Benchmarking the conductor-like polarizable continuum model (CPCM) for aqueous solvation free energies of neutral and ionic organic molecules. J Chem Theory Comput 1(1):70–77
69. Frisch MJ, Trucks GW, Schlegel HB, Scuseria GE, Robb MA, Cheeseman JR et al. Gaussian 09, Revision B.01. Wallingford CT: Gaussian09W, Revision A02; Gaussian, Inc; 2009.
70. Delley B (1990) An all-electron numerical method for solving the local density functional for polyatomic molecules. J Chem Phys 92(1):508–517
71. Delley B (2000) From molecules to solids with the DMol 3 approach. J Chem Phys 113(18):7756–7764
72. Perdew JP, Burke K, Ernzerhof M (1996) Generalized gradient approximation made simple. Phys rev Lett 77(18):3865
73. Benedek N, Snook I, Latham K, Yarovsky I (2005) Application of numerical basis sets to hydrogen bonded systems: a density functional theory study. J Chem Phys 122(14):144102
74. Kusama H, Orita H, Sugihara H (2008) TiO_2 band shift by nitrogen-containing heterocycles in dye-sensitized solar cells: a periodic density functional theory study. Langmuir 24(8):4411–4419
75. Zhang G, Bai Y, Li R, Shi D, Wenger S, Zakeeruddin SM et al (2009) Employ a bisthienothiophene linker to construct an organic chromophore for efficient and stable dye-sensitized solar cells. Energy Environ Sci 2(1):92–95
76. Grätzel M (2001) Photoelectrochemical cells. Nature 414(6861): 338–344
77. Preat J, Jacquemin D, Michaux C, Perpète EA (2010) Improvement of the efficiency of thiophene-bridged compounds for dye-sensitized solar cells. Chem Phys 376(1):56–68
78. Mehmood U, Hussein IA, Harrabi K, Ahmed S (2015) Density functional theory study on the electronic structures of oxadiazole based dyes as photosensitizer for dye sensitized solar cells. Adv Mater Sci Eng 2015:286730
79. Nalwa HS (2001) Handbook of advanced electronic and photonic materials and devices: semiconductors. Vol. 1. San Diego, CA, Academic Press.
80. Wang J, Li H, Ma N-N, Yan L-K, Su Z-M (2013) Theoretical studies on organoimido-substituted hexamolybdates dyes for dye-sensitized solar cells (DSSC). Dyes Pigments 99(2):440–446
81. Pearson RG (1988) Absolute electronegativity and hardness: application to inorganic chemistry. Inorg Chem 27(4):734–740. doi:10.1021/ic00277a030
82. Scharber MC, Mühlbacher D, Koppe M, Denk P, Waldauf C, Heeger AJ et al (2006) Design rules for donors in bulk-heterojunction solar cells—towards 10% energy-conversion efficiency. Adv Mater (Weinheim, Ger) 18(6):789–794